Available online at www.sciencedirect.com

SciVerse ScienceDirect

Ceramics International 39 (2013) 6165–6174

CERAMICS INTERNATIONAL

www.elsevier.com/locate/ceramint

Structural and dielectric properties of $Bi_{1-x}Sr_xMnO_3$ $(0.40 \leq x \leq 0.55)$

Samita Thakur, O.P. Pandey, K. Singh*

School of Physics & Materials Science, Thapar University, Patiala147004, Punjab, India

Received 21 October 2012; received in revised form 12 January 2013; accepted 12 January 2013
Available online 23 January 2013

Abstract

In order to study the effect of Sr substitution on structural and dielectric properties of $Bi_{1-x}Sr_xMnO_3$ $(0.40 \leq x \leq 0.55)$ compounds were synthesized by the solid state reaction method. The as-prepared samples were characterized by X- ray diffraction (XRD) and dielectric measurements to correlate structural changes with dielectric properties. The XRD data were further analyzed by the Rietveld refinement. The highest dielectric constant was observed in $Bi_{0.55}Sr_{0.45}MnO_3$ and $Bi_{0.5}Sr_{0.5}MnO_3$ systems ($\sim 10^6$) mainly because of orientation polarization. The charge ordering temperature decreases with increasing Sr concentration in $Bi_{1-x}Sr_xMnO_3$ systems.

Keywords: B. Rietveld refinement; B. X-ray diffraction (XRD); C. Ac and dc conductivity; C. Dielectric constant

1. Introduction

Electroceramics with high dielectric constant can be used for capacitors and memory devices depending upon the required frequency and temperature range. For capacitive and memory devices, in spite of magneto-electric effects, ceramics should have high dielectric constants. In literature, lots of reports have appeared to explain the origin of high dielectric constant in perovskite structured materials [1,2]. The most probable reason for high dielectric constant is its open structure and presence of non stoichiometry defects [3]. In addition to this, the oxygen vacancies also play a crucial role in relaxation and transport phenomenon. Out of these materials, Sr doped perovskites like ($Ln_{1-x}Sr_xMnO_3$) have attracted the attention of many researchers because of their high dielectric constant, Colossal magnetoresistance (CMR) and charge ordering phenomenon [4]. In these manganites, different oxidation states of Mn play very important role for high dielectric constants. The different oxidation states of Mn in $BiMnO_3$ system depend on the chemical nature of dopants, site occupancy and its magnitude. It has been observed that higher substitution of Sr^{2+} in $La_{1-x}Sr_xMnO_3$ system may lead to the charge ordering [5]. Similar behaviour has also been reported in $Bi_4V_2O_{11}$ systems [6]. The most important problem associated with $Ln_{1-x}Sr_xMnO_3$ is low charge ordering temperature which restricts their usage in electronic industry. On the other hand, $Bi_{1-x}Sr_xMnO_3$ have shown the high charge ordering temperature ($T_o \sim 525$ K) as compared to other rare-earth mixed valence manganites. High charge ordering temperature is related to the electronic structure of Bi^{3+} which have a highly polarisable $6s^2$ lone pair [7]. This high T_o makes this system an interesting candidate for the dielectric studies.

The substituted and non-substituted bismuth based manganites systems have been investigated for their unique magnetic properties. However, very few reports have appeared in the literature related to their dielectric properties [8,9]. Most of these studies are related to $Bi_{0.5}Sr_{0.5}MnO_3$ systems [10]. However, to the best of our knowledge nobody has reported the study by taking Sr^{2+} substituent in different concentrations in these systems. Therefore, we have selected $Bi_{1-x}Sr_xMnO_3$ ($x=0.40$, 0.45, 0.50 and 0.55) systems to understand their dielectric response, ion transport behaviour and relaxation behaviour systematically. The information regarding

*Corresponding author. Tel.: +91 1752393130; fax: +91 1752393005.
E-mail address: kusingh@thapar.edu (K. Singh).

0272-8842/$ - see front matter © 2013 Elsevier Ltd and Techna Group S.r.l. All rights reserved.
http://dx.doi.org/10.1016/j.ceramint.2013.01.035

relaxation mechanism and conductivity has been derived from frequency dependent dielectric spectroscopy. Measurement of frequency dependent conductivity and permittivity not only provide information on steady state transport but also reflect at high frequency transient dielectric response resulting from localized displacement of ions [11].

2. Experimental details

The polycrystalline samples of $Bi_{1-x}Sr_xMnO_3$ ($x=0.40$, 0.45, 0.50 and 0.55) were prepared by conventional solid state reaction method. The stoichiometric compositions of high purity ($>99.98\%$) Bi_2O_3, $MnCO_3$ and $SrCO_3$ powders were mixed thoroughly in an agate mortar pestle for 2 h in acetone media to obtain homogeneous powder. The resulting ground mixtures were dried and calcined in air at 750 °C for 12 h. The calcined powders were again ground and palletized into circular discs of diameter 20 mm by applying 10 t of pressure. The as-prepared pellets were given double stage heat treatment. First, the pellets were sintered at 1050 °C for 12 h. The sintered pellets were ground, compacted and resintered at 1200 °C. This was done to ensure complete homogeneity and good sintered density. The as sintered samples were characterized using X-ray diffraction to identify the formed phases. X-ray powder diffraction study was performed at room temperature using PANalytical X'Pert PRO system with Ni-filter. The XRD data were refined by Rietveld refinement using Fullprof setup. During experiment the step size was 0.013°/min. Dielectric characterization was done by using automated LCR meter (Agilent 4284A precision LCR) in the frequency range of 20–10^6 Hz over temperature range of 30–280 °C. For dielectric studies, the samples were polished, cleaned and sputtered by gold to ensure good electrical contact with electrode. The generated dielectric data was used to calculate the electric modulus, ac and dc conductivities of as prepared samples.

3. Results and discussion

3.1. X-ray diffraction

The density of the sintered samples was calculated using mass to volume ratio of the pellets. The relative density of all the samples is higher than 95% of the theoretical density. The XRD patterns of all the samples are shown in Fig. 1(a–d). The XRD data of these samples exhibit single phase with a tetragonal structure having space group *P4mm*. The XRD results are consistent with the earlier reported structure of $Bi_{1-x}Sr_xMnO_3$ [12,13]. The XRD results are also refined by using Fullproof setup and the parameters are well fitted with $\aleph^2 \leq 2$. All the refined parameters are tabulated in Table 1. As Sr dopant concentration increases, the lattice parameter along *a* and *b* direction (basal plane) decreases marginally from 3.91 to 3.89 Å. In contrast to *a* and *b* lattice parameters, *c* parameter decreases from 3.81 to 3.78 Å upto $x=0.50$

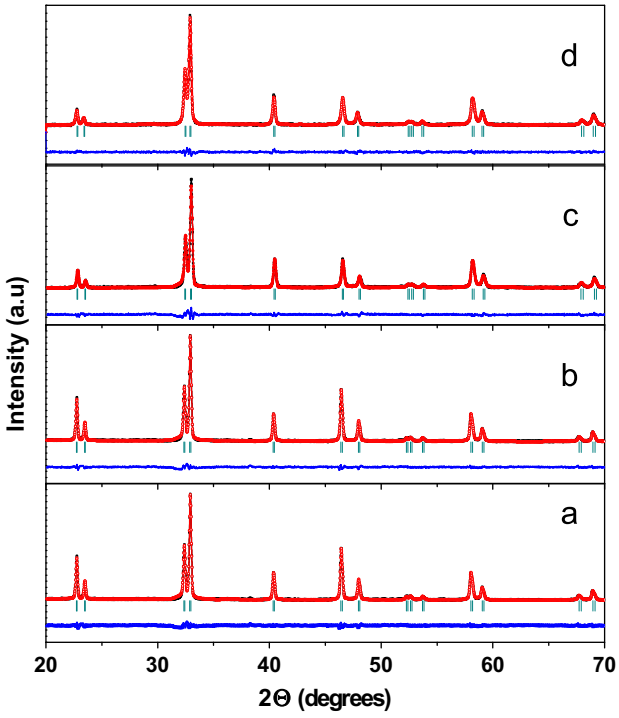

Fig. 1. XRD pattern of $Bi_{1-x}Sr_xMnO_3$ (a) $x=0.40$, (b) $x=0.45$, (c) $x=0.50$, (d) $x=0.55$.

and after that increases for $x=0.55$. Overall, the unit cell volume decreases with the increase in concentration of Sr^{2+} as shown in Fig. 2. It is inconsistent with the reported lattice parameter for $Bi_{0.5}Sr_{0.5}MnO_3$ system [12]. These changes in lattice parameter are unexpected since ionic radii of Sr^{2+} (1.18 Å) is greater than Bi^{3+} (1.03 Å) cation. Munoz et al. [8] have reported that bismuth $6s^2$ lone pair can be the origin of this lattice distortion. With the increase of Sr^{2+} concentration, Bi^{3+} concentration decreases which weaken the local distortion due to the Bi^{3+} lone pair that may decrease *a* and *b* lattice parameters. Therefore, Sr^{2+} substitution not only affects the hole carrier density but also the strength due to local distortion in the unit cell. In addition to this, another possible reason for lattice parameter anomalies is the creation of oxygen vacancies as well as the change in oxidation state of Mn^{3+} (0.58 Å) to Mn^{4+} (0.53 Å) or higher than this to compensate the charge in the overall system. It is well reported in the literature that Mn^{3+} gets converted to the higher oxidation state above 600 °C during processing [14].

3.2. Dielectric properties

The frequency response of dielectrics to sinusoidal electric fields can be expressed by their complex relative dielectric permittivity as follows:

$$\varepsilon_r(w) = \varepsilon_r'(w) - i\varepsilon_r''(w) \quad (1)$$

where $i=\sqrt{-1}$ and $\varepsilon_r = \varepsilon/\varepsilon_0$ (ε_0 is free space permittivity) and w is angular frequency; ε_r' is the real component,

Table 1
Refined structural parameters for $Bi_{1-x}Sr_xMnO_3$.

Composition	Wyckoff positions	Atom	X	y	Z	χ^2
$Bi_{0.60}Sr_{0.40}MnO_3$ (*P4mm*) $a=b=3.915076$ Å, $c=3.815839$ Å	1a	Bi/Sr	0	0	0	1.7
	1b	Mn	0.5	0.5	0.54436	
	1a	OI	0.5	0.5	0.154770	
	2b	OII	0.5	0	0.58350	
$Bi_{0.55}Sr_{0.45}MnO_3$ (*P4mm*) $a=b=3.910704$ Å, $c=3.790831$ Å	1a	Bi/Sr	0	0	0	1.6
	1b	Mn	0.5	0.5	0.45509	
	1a	OI	0.5	0.5	0.10435	
	2b	OII	0.5	0	0.54371	
$Bi_{0.5}Sr_{0.5}MnO_3$ (*P4mm*) $a=b=3.901714$ Å, $c=3.786850$ Å	1a	Bi/Sr	0	0	0	1.8
	1b	Mn	0.5	0.5	0.50378	
	1a	OI	0.5	0.5	0.16705	
	2b	OII	0.5	0	0.60180	
$Bi_{0.45}Sr_{0.55}MnO_3$ (*P4mm*) $a=b=3.895225$ Å, $c=3.792847$ Å	1a	Bi/Sr	0	0	0	1.4
	1b	Mn	0.5	0.5	0.49930	
	1a	OI	0.5	0.5	0.044247	
	2b	OII	0.5	0	0.60753	

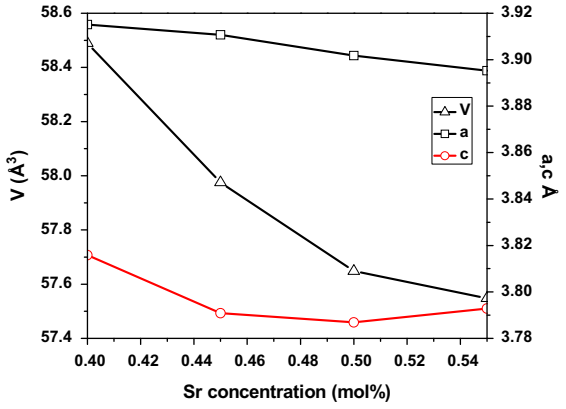

Fig. 2. Variation of lattice constant with respect to Sr concentration.

which is in phase with the applied field and ε_r'' is the imaginary component which is in quadrature with the applied field.

3.2.1. Real part of the dielectric constant

The variation of real part of dielectric constant (ε_r') of different samples with respect to frequency at different temperatures are shown in Fig. 3. The dielectric response of these samples does not show any peak related to the losses which clearly indicates that the polarization in this system is dominated by the hopping mechanism [10]. All the dielectric plots can be divided into three parts: lower frequency region (< 100 Hz), intermediate frequency region (10^3–10^5 Hz) and high frequency region, i.e., above 10^6 Hz. All the samples show high dielectric constant in lower region. After this, the dielectric constant decreases slightly and becomes constant. In the third part dielectric constant again decreases. The decrement in dielectric constant at high frequency is in steps. The same behaviour is observed in $La_{1-x}Sr_xMnO_3$ and $CaCu_3Ti_4O_{12}$ systems by other researchers [15,16]. These different steps may arise due to the electrode, grains and grain boundary contributions. The dielectric behaviour of these samples at low frequencies can be explained on the basis of extrinsic interfacial Maxwell–Wagner model [17]. According to this model the dispersion of ε_r' at low frequencies is due to interfacial polarization and existence of depletion layers near the sample-electrode contacts. Second, the electrical charge unbalance caused by the divalent Sr^{2+} ion substitution for the trivalent Bi^{3+} ions is compensated by the creation of the oxygen vacancies as well as transition of Mn^{3+} to Mn^{4+} at the octahedral sites. It could be suggested that due to the ionization of oxygen vacancies, hopping of electrons may contribute to the dielectric relaxation process in these samples. The samples show high values of dielectric constant for frequencies lower than 10^3 Hz. This is a clear indication that within a single material two types of dispersion mechanisms are present, one of which dominates at higher frequencies. This behaviour resembles the Debye relaxation and in this region ε_r' varies as (w^{m-1}) [17]. $Bi_{0.60}Sr_{0.40}MnO_3$ shows very small dielectric constant as compared to the other samples. In this particular sample, Sr content is low as compared to other samples, so it may be the reason that low Sr concentration created smaller number of oxygen vacancies as well as low conversion of Mn^{3+} to Mn^{4+} which may lead to less distortion in the lattice as compared to higher Sr^{2+} substituted samples. Consequently, it has smaller dielectric constant as compared to $x=0.45$ and $x=0.50$ samples. Second, it is possible that higher ordering of oxygen vacancies in these samples is taking place. This type of phenomenon is very common in doped ceramic samples and well reported in literature [6]. Additionally, the low content of oxygen vacancies in $x=0.40$ sample may be responsible for the low concentration of hopping charge carriers. $Bi_{0.55}Sr_{0.45}MnO_3$ and $Bi_{0.50}Sr_{0.50}MnO_3$ show higher values of dielectric constant which is due to creation of higher number of oxygen vacancies as well as

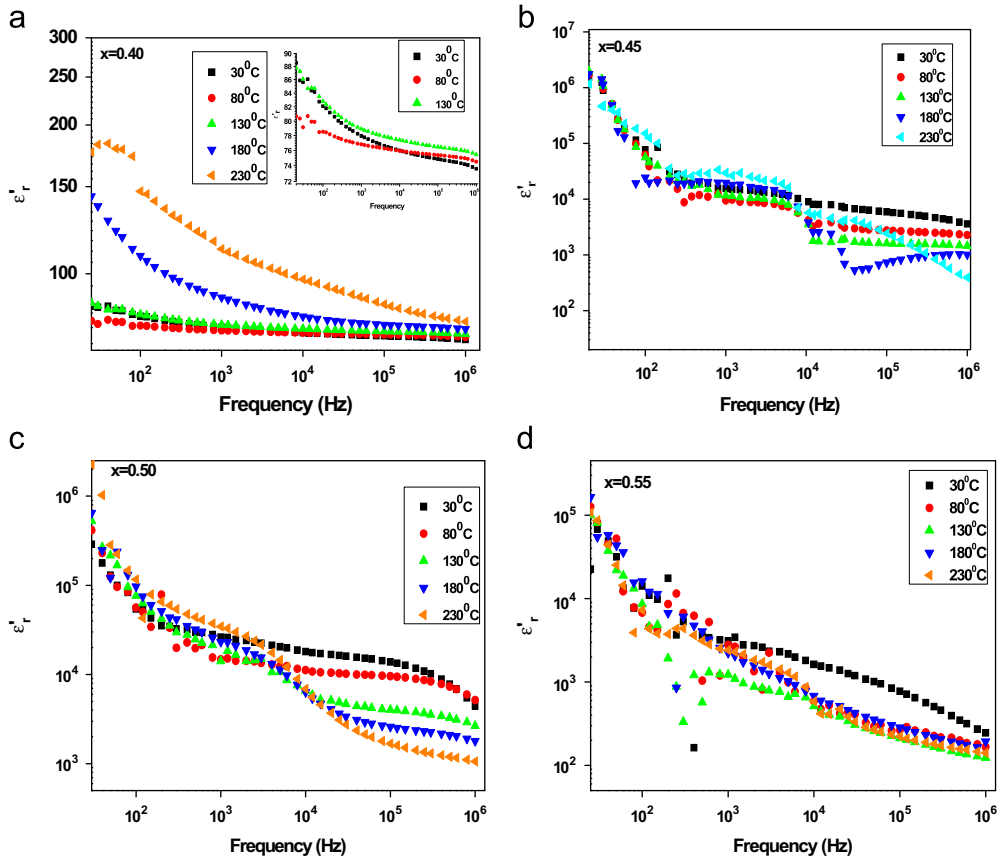

Fig. 3. Variation of ε_r' with respect to frequency at different temperatures for $Bi_{1-x}Sr_xMnO_3$ (a) $x=0.40$ (b) $x=0.45$ (c) $x=0.50$ and (d) $x=0.55$.

high conversion of Mn^{3+} to Mn^{4+} in these samples as compared to other samples. Furthermore, $Bi_{0.45}Sr_{0.55}MnO_3$ again show a decrease in dielectric constant that may be due to the ordering in crystal lattice above $x=0.50$. The dielectric constant is not much dependent on the temperature at low frequencies ($<10^3$ Hz) except $x=0.40$. But at high frequencies (10^3–10^6 Hz), as the temperature increases the dielectric constant decreases. Basically, in the present samples the temperature plays two-fold effect, if orientation polarization is dominated in the system then the temperature randomize it and tend to decrease the dielectric constant. Consequently, the overall dielectric constant is going to decrease in the system. On the other hand, if polarization is predominantly governed by the space polarization then dielectric constant of the system is going to increase with increasing temperature because the rate of interfacial charge accumulation increases. Conclusively, the present samples exhibit the orientational polarization predominantly [18]. Moreover, at low frequencies, the dielectric is mainly because of the movement of free charges which increases with the rise in temperature and further increases the value of dielectric constant. But at the high frequencies and high temperature, dispersion losses increase due to the thermal vibrations and less time is available for the materials to respond for the applied electric field. Variation of real part of dielectric constant ε_r' with respect to temperature is also shown in Fig. 4 at

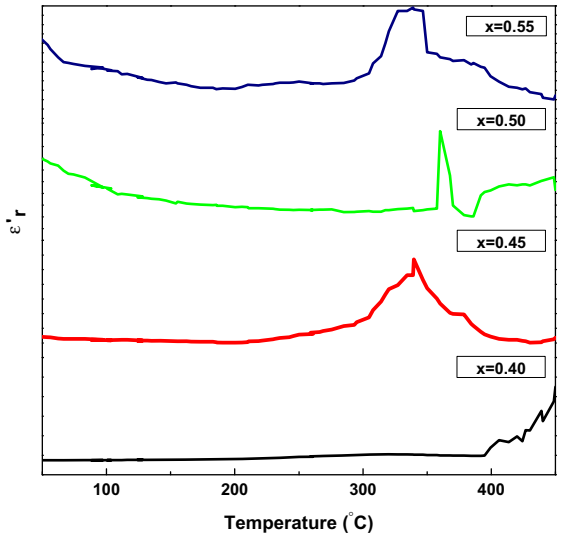

Fig. 4. Variation of ε_r' with temperature for $Bi_{1-x}Sr_xMnO_3$.

10 kHz. The curves show maxima in the range of 280–350 °C. As the frequency increases, maxima shift to higher values of temperature. This temperature range corresponds to the charge ordering temperature of these compounds [12,13]. This charge ordering can be described as Mn^{3+}/Mn^{4+} separation/ ordering in the ionic systems. $Bi_{1-x}Sr_xMnO_3$ has a high charge ordering temperature as

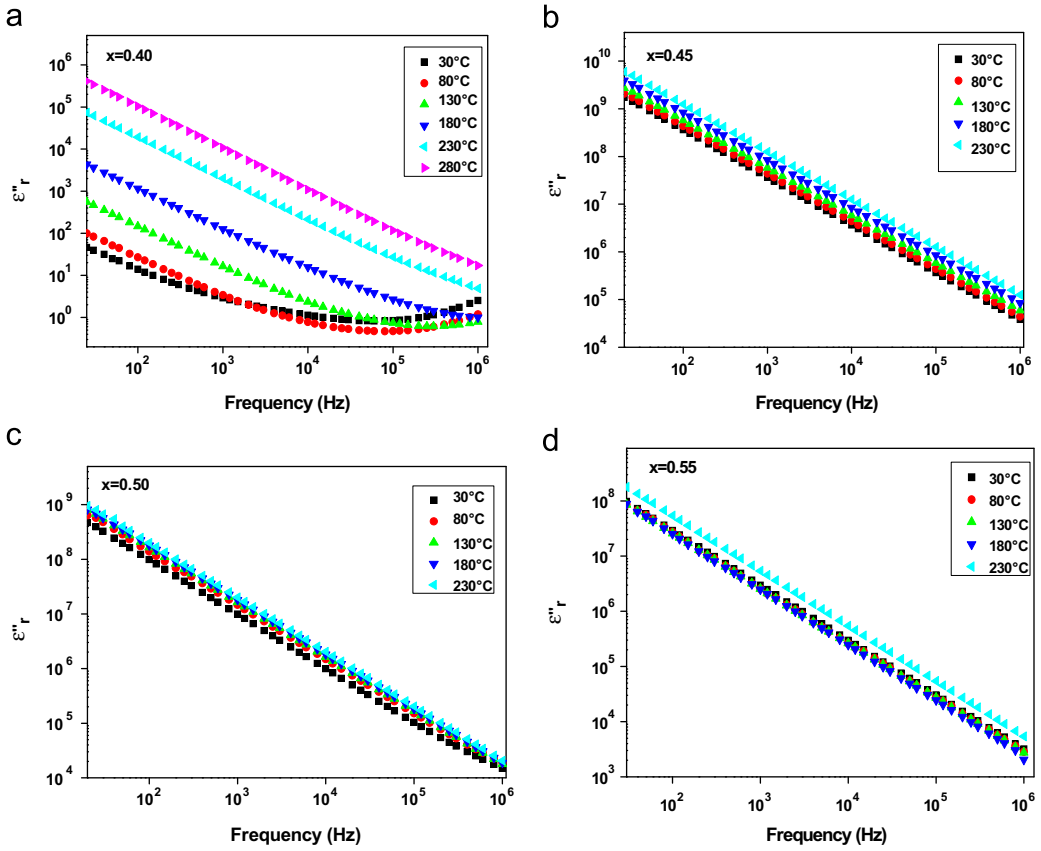

Fig. 5. Variation of ε_r'' with frequency in $Bi_{1-x}Sr_xMnO_3$ (a) $x=0.40$ (b) $x=0.45$ (c) $x=0.50$ and (d) $x=0.55$.

compared to other manganites [9]. This high T_o can be attributed to the electronic structure of Bi^{3+}, which has $6s^2$ lone pairs in its outermost shell and these electrons have strong p-character in these compounds. This lone pair hybridizes with oxygen p-orbitals lowering the mobility of Mn electrons and favours the charge ordering and charge localization. Thus T_o decreases with increasing content of dopant [8].

3.2.2. Imaginary part of dielectric constant

The frequency dependence of imaginary part of dielectric constant (ε_r'') of all the compounds are shown in Fig. 5. It can be seen that in all the samples ε_r'' shows higher values except for $Bi_{1-x}Sr_xMnO_3$ ($x=0.40$) that increases as temperature increases and decreases as frequency increases. As a result, these samples exhibit high losses as can be observed from the variation of tan δ versus frequency at different temperatures. In $x=0.40$, ε_r'' shows minima in the frequency range 10^4–10^5 Hz which shifts to higher frequencies as temperature increases. In the case of other samples, ε_r'' vary from 10^{10} to 10^4 in the frequency range of 20–10^6 Hz. In the low frequency region, all the samples show higher values of losses and $\varepsilon_r''(w) > \varepsilon_r'(w)$. This part of dielectric losses follows w^{-1} dependence according to the electrodynamics relation $\varepsilon''(w) = \sigma_{dc}/\varepsilon_0 w$ [19]. Thus, in this frequency region dc conductivity might dominate. With increasing temperature, conductivity increases in ionic solids which further increases the losses as can be seen from ε_r'' versus frequency curve in Fig. 5. For $x=0.45$, 0.50 and 0.55 the ε_r'' curves are straight line for complete test frequency range and varies as w^{-1} which clearly indicates that the conductivity losses for all the samples dominate due to dc conductivity.

3.2.3. Dielectric losses

The variation of tan δ with frequency at different temperatures is shown in Fig. 6. Tan δ varies in the range of 10^4 to 10^{-2} for all the samples in the frequency range of 20–10^6 Hz. At lower frequencies ($< 10^2$ Hz) tan δ have high values. In the case of $x=0.40$, as the frequency increases the values of tan δ decreases in the frequency range 10^2–10^5 Hz, after that it becomes almost constant in the higher frequency range $> 10^5$ Hz. The decrease in tan δ corresponds to plateau like behaviour as observed in ε_r' versus frequency curve. As the temperature increases the tan δ values also increases. Tan δ show a minima in the frequency range 10^5–10^6 Hz and minima shifts to higher frequencies with increase in temperature. All these losses are due to the conductivity losses as explained in previous section. In $x=0.45$, 0.50 and 0.55 tan δ curves show two shallow peaks; one at very low frequencies (< 100 Hz) and another at high frequency (< 1000 Hz). The low frequency peak originates due to the interfacial polarization. On the

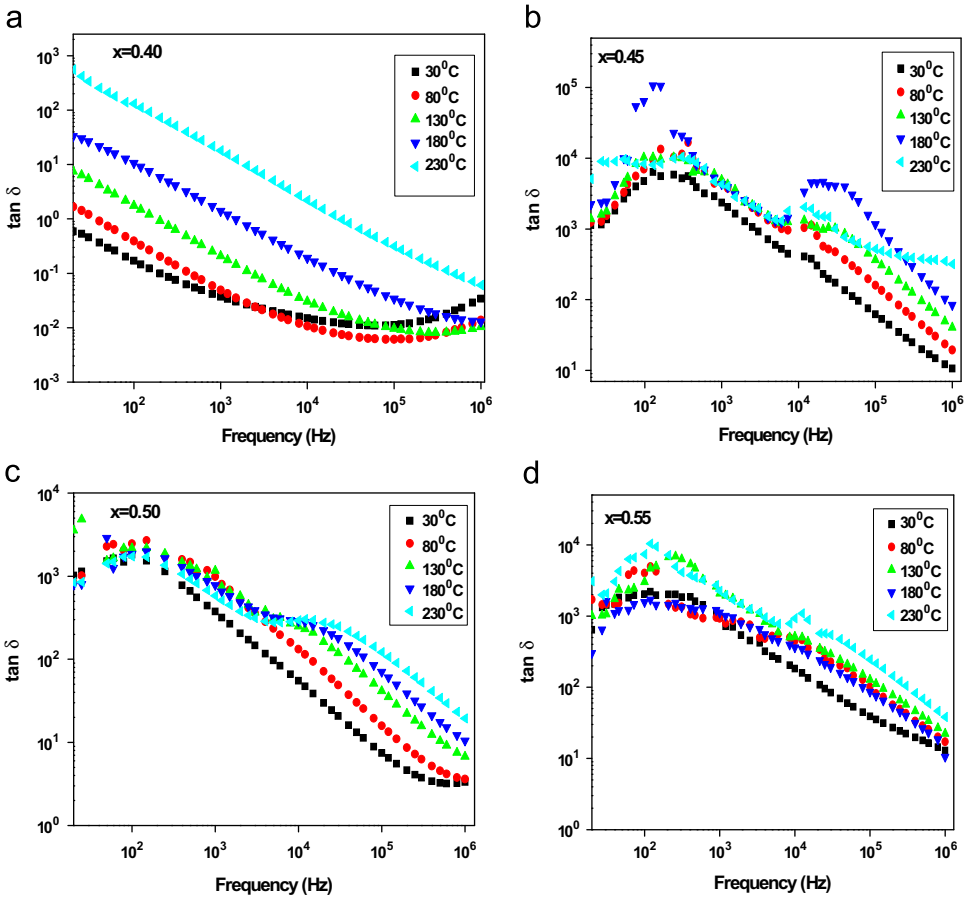

Fig. 6. Variation of tan δ with frequency in $Bi_{1-x}Sr_xMnO_3$: (a) $x=0.40$, (b) $x=0.45$, (c) $x=0.50$ and (d) $x=0.55$.

other hand, second peak is related to the dc conductivity losses at high frequencies.

3.3. Electric modulus

The electric modulus $M^*(w)$ can be expressed as:

$$M^* = \frac{1}{\varepsilon^*} = M'(w) + iM''(w) = M_\infty \left[1 - \int_0^\infty e^{-iwt} \frac{d\emptyset(t)}{dt}\right] \quad (2)$$

where the function $\emptyset(t)$ gives the time variation of electric field within dielectric. Real part $M'(w)$ and imaginary parts $M''(w)$ of the electric modulus are related to dielectric constant as follows:

$$M'(w) = \frac{\varepsilon'(w)}{\varepsilon'(w)^2 + \varepsilon''(w)^2} \quad \text{and} \quad M''(w) = \frac{\varepsilon''(w)}{\varepsilon'(w)^2 + \varepsilon''(w)^2} \quad (3)$$

As discussed in the results of ε_r' and ε_r'' with respect to frequency in Figs. 3 and 5, it clearly indicates that ε_r' and ε_r'' increases with increase in temperature at low frequency region, which may be related to the conduction process in these samples. In order to discuss this phenomenon in detail, the values of dielectric constant is converted into imaginary parts of electric modulus by using Eq. (3) and the as obtained values are given in Fig. 7 for all the samples. From Fig. 7, it is clear that M'' values are very small at lower frequencies indicating the removal of electrode polarization [20]. The values of M'' show decreasing trend with increasing temperature. This may be due to the increase in the mobility of charge carriers and orientation of the molecular dipoles with the temperature which further increases the conductivity and decreases the electric modulus values. The peak values of M'' depend only on the temperature, which implies that capacitances of grains and grain boundaries depend weakly upon temperature. At higher frequencies sharp peaks are observed for $x=0.40$ and these peaks shift to higher frequency side with increasing temperature. The low frequency side of the peak represents the range of frequencies in which charge carriers can move over long distances. The high frequency side of the peak represents the range of frequencies in which the charge carriers are spatially confined to their potential wells and thus could make localized motion within the potential well. The frequency region where peak is observed represents the transition from long range to the short range mobility of the carriers. The broadening of the peaks with rise in temperature indicates the increase in non-Debye behaviour [21]. For other samples $x=0.45$, 0.50, 0.55 the M'' shows very low values up to $>10^5$ Hz frequency range. This may be due to the high conductivity values of these samples as compared to $x=0.40$ sample. The frequency (f_{max}) corresponding to maxima of each peak is known as relaxation frequency and gives the most probable conductivity relaxation time for ions. The variation τ versus temperature is shown in Fig. 6a. The curve satisfies the Arhenius behaviour with activation energy 0.59 eV. The rise in

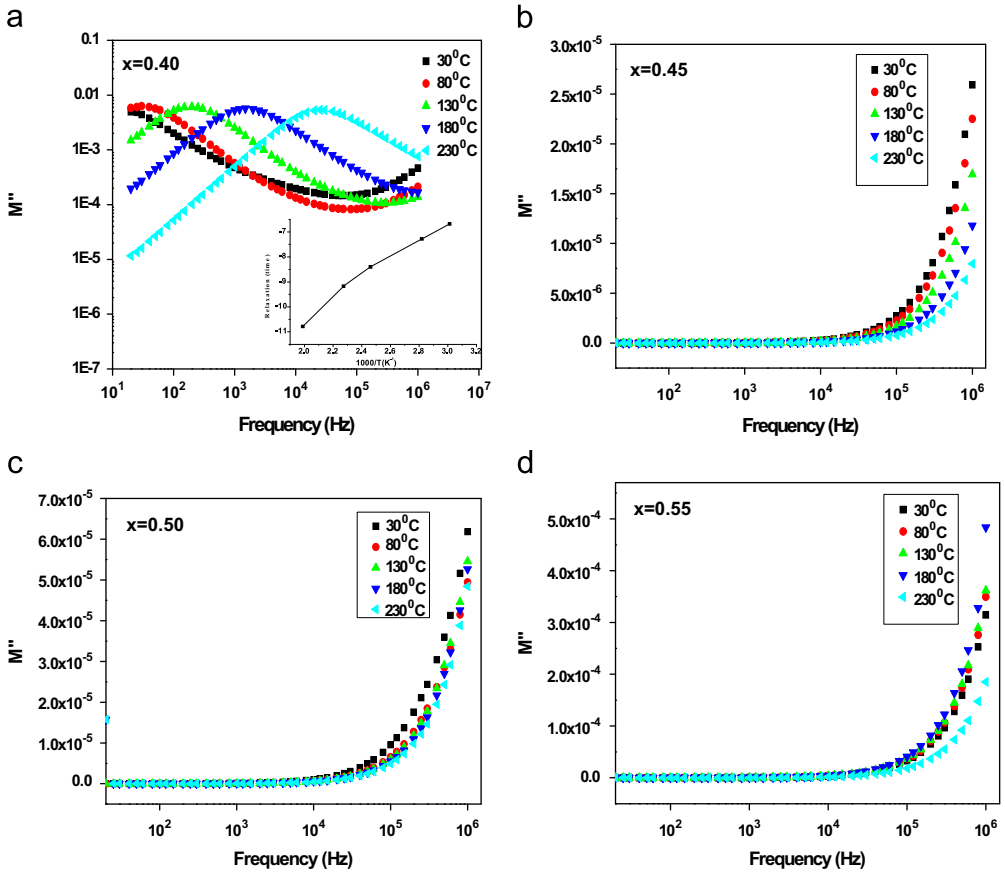

Fig. 7. Variation of electric modulus (M'') with frequency in $Bi_{1-x}Sr_xMnO_3$: (a) $x=0.40$, (b) $x=0.45$, (c) $x=0.50$ and (d) $x=0.55$.

temperature causes a drop in relaxation time due to the increased mobility of ionic carriers.

3.4. Electrical conductivity analysis

3.4.1. Frequency dependent conductivity

The ac conductivity has been calculated from real part of dielectric constant and dielectric loss by using the relation

$$\sigma(w) = \varepsilon_0 w\varepsilon'' = \varepsilon_0 w\varepsilon' \tan\delta \quad (4)$$

The frequency dependence of ac conductivity (σ_{ac}) is shown in Fig. 8. The ac conductivity was found to be frequency independent in the low frequency region suggesting that the ionic diffusion is random. As frequency exceeds from hopping frequency, the conductivity increases and follow the universal power law $\sigma(w)\alpha w^n$ for $x=0.40$ and $x=0.50$ [10]. On the other side $x=0.45$ and $x=0.55$ samples do not show any variation in conductivity with respect to frequency at different temperatures. With increase in temperature these plateau shifts to high frequency region for $x=0.40$ and $x=0.50$ samples. The ac conductivity behaviour is analysed by using the universal power law [10]:

$$\sigma_{ac} = \sigma_{dc} + Aw^s \quad (5)$$

here $A = \frac{\sigma_{dc}}{w_h^s}$

where A is constant for particular temperature, σ_{dc} is dc conductivity and the exponent s is related to the degree of correlation among moving ions. In general, the value of s varies between 0.6 and 1 for ionic conductors. Ac conductivity spectra for different temperatures were fitted using Eq. (5) and the parameters s, A and σ_{dc} were calculated. The as-obtained values of s and A have been used to calculate w_h. w_h is hopping frequency which is defined as the crossover frequency from dc to the dispersive region of ac conductivity.

For $x=0.40$, at low and high frequency region, Eq. (5) gives different results up to 180 °C. For lower frequencies, s varies between 0.81 and 0.45 in the temperature range of 30–230 °C. This power law frequency dependence indicates that the ac conductivity in the low temperature region corresponds to short range hopping of localized charge carriers through trap sites separated by potential barriers and thus it is hopping type conduction. At higher frequencies, the value of s varies between 1.75 and 1 in the temperature range of 30–180 °C. In this frequency range $s>1$ and the system follows the super linear power law (SLPL) which may account for the resonance like effect between the external electrodes and the sample [22]. Similarly, an abrupt increase is also observed in ε'' versus frequency curve for $x=0.40$. For $x=0.50$, value of s varies between 0.5 and 0.9 in the temperature range of 30 –280 °C which is again well fitted with the universal power law.

3.4.2. Temperature-dependent conductivity

The variation of σ_{dc} and w_h versus temperature are shown in Figs. 9 and 10 for all the samples. The conductivity pattern

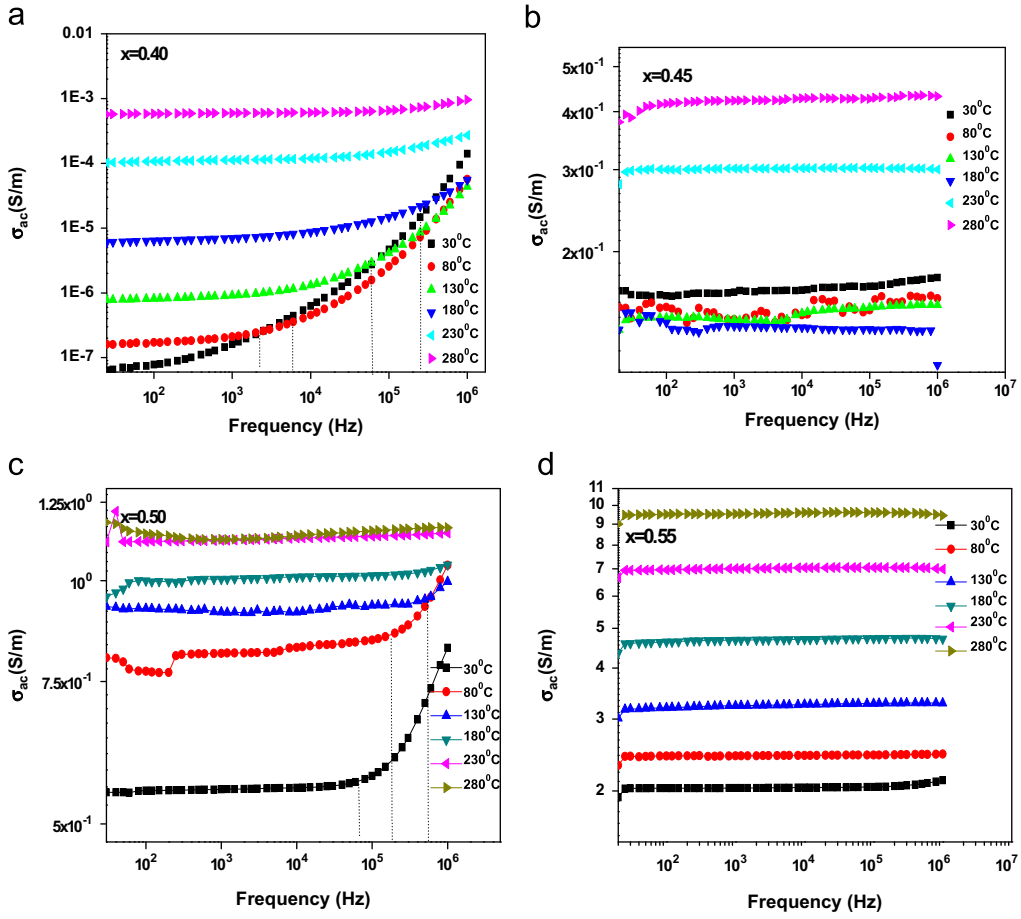

Fig. 8. Variation of conductivity (σ) with frequency in $Bi_{1-x}Sr_xMnO_3$: (a) $x=0.40$, (b) $x=0.45$, (c) $x=0.50$ and (d) $x=0.55$.

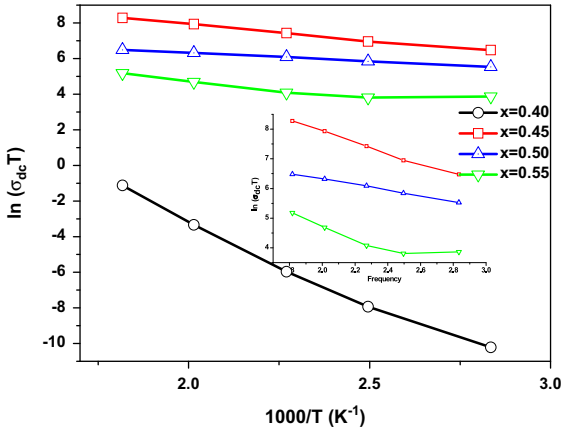

Fig. 9. Arhenius plot of dc conductivity (σ_{dc}).

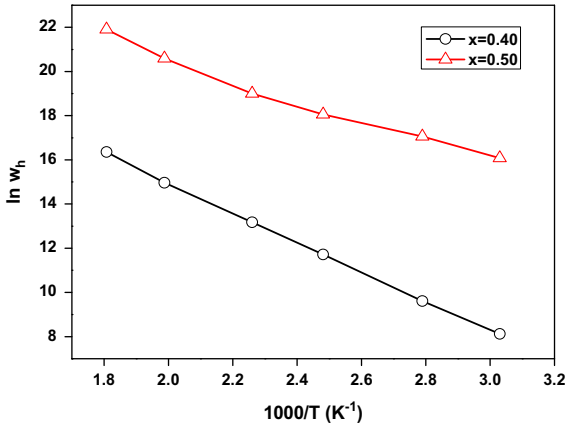

Fig. 10. Arhenius plot of hopping frequency (w_h).

shows an increase in conductivity with temperature. Temperature dependence of conductivity clearly indicates that conduction is a thermally activated process in all the samples. These spectra are fitted with the Arhenius equation as follows:

$$\sigma_{dc}T = \sigma_0 \exp\left(\frac{-E_\sigma}{kT}\right) \quad (6)$$

$$w_h = w_0 \exp\left(\frac{-E_h}{kT}\right) \quad (7)$$

where σ_0 is the dc conductivity pre-exponential factor, k is the Boltzman's constant, E_σ is dc conduction activation energy for mobile ions, w_0 is pre-exponential factor for hopping frequency, E_h is activation energy for hopping frequency. The activation energies calculated from Eqs. ((6) and (7)) are shown in Table 2. Based on these results, it can

Table 2
Activation energies of dc, ac and hopping frequency.

Sample composition $Bi_{1-x}Sr_xMnO_3$	$E_{a(dc)}$ (eV)	$E_{a(ac)}$ (eV)	$E_{a(w_h)}$ (eV)
$x=0.40$	0.68	0.62	0.57
$x=0.45$	0.14	0.11	–
$x=0.50$	0.06	0.07	0.40
$x=0.55$	0.08	0.096	–

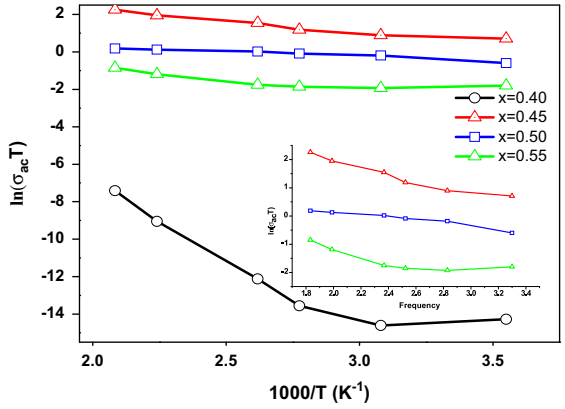

Fig. 11. Arhenius plot of ac conductivity (σ_{ac}) for $Bi_{1-x}Sr_xMnO_3$.

be concluded that the jumps of localized charge carriers from one trap site to another are a thermal driven and random process in theses samples.

Ac conductivity versus temperature spectra are shown in Fig. 11. These spectra are also fitted with the Arhenius equation $\sigma_{ac}T=\sigma_{0ac}\exp(-E_{\sigma ac}/kT)$ and activation energies calculated for all the samples are tabulated in Table 2. The same values of E_{dc} and E_{ac} for all samples may imply the similar origin corresponding to dc and ac conductivity; means similar localized charge carriers are involved in both the conduction phenomenon. Small values of activation energies also indicate that there is mainly electronic conduction in the samples [23]. Even for $x=0.40$, E_h is also very close to the values of ac and dc activation energies which also confirms the similar origin of ac and dc conductivities in the present sample.

4. Conclusion

The Rietveld refinement confirms the tetragonal crystal symmetry in the present samples. The unit cell volume decreases with the increasing concentration of Sr^{2+} in the system. Dielectric constant of all the present samples is in the range of 10^6 with high dielectric losses except for $Bi_{0.6}Sr_{0.4}MnO_3$. The dc conduction in these samples is mainly responsible for these losses. The charge ordering temperature is observed in the range of 280–300 °C. The activation energies and Arhenius plot behaviour suggest the predominant ionic conduction in $x=0.40$ sample. Contrary to this, $x=0.45$, 0.50 and 0.55 samples exhibit very low activation energies ≤ 0.14 eV.

Acknowledgement

Authors are thankful to Defence Research and Development Organisation (DRDO) vide letter no. ERIP/ER/1103976/M/01/1411 for financial support. The authors also thank to Mr. Ravi Shukla, Thapar University, Patiala for the dielectric measurements and Mr. Paramjyot Jha, Thapar University, Patiala for XRD measurements.

References

[1] M.A. Subramanian, Li Dong, N. Duan, B.A. Reisner, A.W. Sleight, High dielectric constant in $ACu_3Ti_4O_{12}$ and $ACu_3Ti_3FeO_{12}$ phases, Journal of Solid State Chemistry 151 (2000) 323–325.
[2] P. Raevski, S.A. Prosandeev, A.S. Bogatin, M.A. Malitskaya, L. Jastrabik, High dielectric permittivity in $AFe_{1/2}B_{1/2}O_3$ nonferroelectric per-ovskite ceramics (A=Ba, Sr, Ca; B=Nb, Ta, Sb), Journal of Applied Physics 93 (2003) 4130–4136.
[3] I. Reiss, Mixed ionic–electronic conductors-material properties and applications, Solid State Ionics. 157 (2003) 1–17.
[4] Y. Tokura, Y. Tomioka, Colossal magnetoresistive manganites, Journal of Magnetism and Magnetic Materials 200 (1999) 1–23.
[5] Y. Yamada, O. Hino, S. Hondo, R. Kanao, Polaron ordering in low-doping $La_xSr_xMn0_3$, Physical Review Letters 77 (1996) 904–907.
[6] Ravi Kant, K. Singh, O.P. Pandey, Structural and ionic conductive properties of $Bi_4V_{2-x}Ti_xO_{11-\delta}$ $(0\leq x\leq 0.4)$ compound, Materials Science and Engineering B 158 (2009) 63–68.
[7] S. Yamada, T. Matsunaga, E. Sugano, H. Sagayama, S. Konno, S. Nishiyama, Y. Watanable, Phase diagram and anisotropic physical properties of single crystal $Bi_{1-x}Sr_xMnO_3$ $(0.35\leq x\leq 0.64)$, Arima, Physical Review B: Condensed Matter 75 (2007) 214431(1)–214431(7).
[8] J.L. García-Muñoz, C. Frontera, Rivas-Murias, J. Mira, Dielectric properties of $Bi_{1-x}Sr_xMnO_3$ (x=0.40,0.50) manganites: influence of room temperature charge order, Journal of Applied Physics 105 (2009) 084116(1)–084116(5).
[9] D.L. Sodebottom, C.M. Murray-Krezan, Properties of the near constant loss in selected phosphate and germanate glasses, Physical Review Letters 89 (2002) 195901–195904.
[10] J.L. Gracia-Munoz, C. Frontera, M.A.G. Aranda, A. Llobet, C. Ritter, High-temperature orbital and charge ordering in $Bi_{1/2}Sr_{1/2}MnO_3$, Physical Review B: Condensed Matter 63 (2001) 064415(1)–064415(4).
[11] A.K. Jonscher, Dielectric Relaxation in Solids, Chalesa Dielectric Press, London, 1983.
[12] B.H. Kim, J.S. Kim, M.S. Kim, C.J. Zhang, K.H. Kim, B.G. Kim, H.C. Kim, Y.W. Park, High temperature charge ordering in Bi1−xSrxMnO3 $(0.45\leq x\leq 0.8)$, Physics Letters A 351 (2006) 368–372.
[13] H. Chiba, Y. Atou, Y. Syono, Magnetic and electrical properties of $Bi_{1-x}Sr_xMnO_3$: hole-doping effect on ferromagnetic provskite $BiMnO_3$, Journal of Solid State Chemistry 132 (1997) 139–143.
[14] S.P. jiang, Development of lanthanum strontium manganite perovskite cathode materials of solid oxide fuel cells: a review, Journal of Materials Science. 43 (2008) 6799–6833.
[15] M.P. Gutierrez, J. Mira, J. Rivas, Influence of charge-ordering on the dielectric response of $La_{1-x}Sr_xMnO_3$, Physics Letters A 323 (2004) 473–476.
[16] R.K. Raman Kashyap, O.P. Mishra, Thakur, R.P. Tandon, Structural, dielectric properties and electrical conduction behaviour of Dy substituted $CaCu_3Ti_4O_{12}$ ceramics, Ceramics International 38 (2012) 6807–6813.
[17] K.Andrew Jonscher, Dielectric relaxation in solids, Journal of Physics D: Applied Physics 32 (1999) R57–R70.

[18] V. Raghvan, Materials Science and Engineering, PHI Learning Private Limited, New Delhi, 2010.
[19] Dutta, T.P. Sinha, P. Jena, S. Adak, Ac conductivity and dielectric relaxation in ionically conducting soda–lime–silicate glasses, Journal of Non-Crystalline Solids 354 (2008) 3952–3957.
[20] L.N. Patrol, K. Hariharan, Frequency dependent conduction characteristics of mechanochemically synthesized $NaSn_2F_5$, Material Science and Engineering B 162 (2009) 173–178.
[21] J.S. Kim, Electric modulus spectroscopy of lithium tetraborate (Li2B4O7) single crystal, Journal of the Physical Society of Japan 70 (2001) 3129–3133.
[22] R. Thomas, V.K. Varadan, S. Komarneni, D.C. Dube, Diffuse phase transitions, electrical conduction, and low temperature dielectric properties of sol–gel derived ferroelectric barium titanate thin films, Journal of Applied Physics 90 (2001) 1480–1488.
[23] H. Zhao, W. Shen, Z. Zhu, X. Li, Z. Wang, Preparation and properties of $Ba_xSr_{1-x}Co_yFe_{1-y}O_{3-\delta}$ cathode material for intermediate temperature solid oxide fuel cells, Journal of Power Sources 182 (2008) 503–509.